Methodology matters: characterization of glioma through advanced MR imaging

Schmitz Abecassis, B.

4 Investigation of metabolite correlates of CEST in the human brain at 7T

Bárbara Schmitz-Abecassis
Chloé Najac
Jaimy Plugge
Matthias J. P. van Osch
Ece Ercan

NMR in Biomedicine (2024). DOI: 10.1002/nbm.5104

4.1 Abstract

Metabolite-weighted chemical exchange saturation transfer MRI can be used to indirectly image metabolites such as creatine and glutamate. This study aims to further explore the contrast of CEST at 2 ppm in the human brain at 7T and investigate the metabolite correlates of CEST at 2 ppm via correlations with magnetic resonance spectroscopy (MRS).

Simulations were performed to establish the optimal acquisition parameters, such as total saturation time (t_{sat}) and B_1 root mean squared (B_1rms) for CEST at 2 ppm in the human brain. Parameters were validated via *in vitro* phantom studies at 7T using concentrations, pH and temperature comparable to what is found in the human brain. Finally, 10 healthy volunteers were scanned at 7T for comparison with MRS.

Our results show that the optimal parameters to acquire CEST at 2 ppm images are: B_1rms = 2.14 μT & t_{sat} = 1500 ms, respectively. Comparison with MRS showed no significant correlation between CEST at 2 ppm and total Creatine measured by MRS (R = 0.19; p-value = 0.273). However, a significant correlation was found between CEST at 2 ppm and Glu (R = 0.39; p-value = 0.033), indicating the broad Glutamate-weighted CEST as the main measurable contributor to CEST at 2 ppm.

We identified and confirmed optimal CEST at 2 ppm sequence parameters and validated CEST at 2 ppm measurements in a controlled *in vitro* environment. Our findings suggest that glutamate is a substantial contributor to the CEST at 2 ppm contrast observed in the human brain, whereas the creatine contribution to CEST at 2 ppm in the brain did not show a measurable contribution.

4.2 Introduction

Chemical exchange saturation transfer (CEST) MRI is an emerging technique which allows to non-invasively image endogenous metabolites and proteins *in vivo*[48]. CEST is derived from the exchange of protons between the bulk water pool and the solute pool of interest. CEST contrast is achieved by applying a train of frequency specific RF pulses with a certain B_1 power to saturate the pool of interest and by measuring the decrease in the signal from the water pool due to chemical exchange. CEST is a very sensitive technique for *in vivo* metabolic imaging and highly benefits from ultra-high field (UHF) (e.g. 7T, 9.4T MRI), exploiting the advantage of higher SNR and higher spectral resolution at UHF.

Fast and intermediate exchanging CEST pools of guanidium and amine protons, resonating at approximately 2 and 3 ppm from the water signal, respectively, have gained recent interest given the presence of these protons in metabolites such as creatine (Cr) and glutamate (Glu)[49]. The most popular examples of metabolite-weighted CEST include glutamate-weighted (CEST at 3 ppm) CEST for the brain and creatine-weighted (CEST at 2 ppm) CEST for brain and muscle[90,93–95]. The alteration of CEST at 3 ppm contrast from amine protons has also been investigated in the scope of brain pathologies. Especially in epilepsy, CEST at 3 ppm has shown promise in identifying epileptic foci in patients[96]. Similarly, in brain tumors, Neal et al. have shown increased CEST at 3 ppm in glioma associated epilepsy, specifically in the peritumoral area[45]. CEST at 2 ppm, on the other hand, has mostly been explored for muscle imaging[94]. Preclinical work by Cai et al. has been able to correlate the concentration of Cr and CEST at 2 ppm contrast as an indicator of brain tumor aggressiveness[97].

Differentiating between CEST at 2 ppm and CEST at 3 ppm pools in the brain can be challenging because of the proximity of their resonance spectra. While the exchange rates for CEST at 3 ppm and CEST at 2 ppm, and thus the optimal acquisition parameters for achieving maximum contrast, differ, other factors such as temperature and pH influence the resulting CEST effect[66,98]. The origins of CEST at 3 ppm is for the most part well established, despite a recent study suggesting that CEST at 3 ppm in the rat brain is originating from amines in proteins[92]. Previous work has shown and validated the substantial contribution of glutamate to CEST at 3 ppm contrast in the brain of a similar animal model and of three healthy volunteers[88]. However, limited work is available validating CEST at 2 ppm of the human brain *in vivo* at 7T. The optimal acquisition parameters and metabolite correlates of CEST at 2 ppm in the human brain at 7T is also yet to be established. Although Harris et al. have already investigated the feasibility of CEST at 2 ppm imaging in phantoms, this was not performed in the human brain at 7T. Singh et al. have carried out the phantom experiments at 7T, evaluating the feasibility of CEST at 2 ppm imaging using Z-spectral fittings as well as in a small group of four volunteers. However, phantom experiments did not include T_1 and T_2 corrections to match those of the brain, and the *in vivo* experiments did not include MR spectroscopy (MRS) validation to confirm the origins of CEST at 2 ppm or correlate the CEST at 2 ppm contrast with Cr concentration[89].

The aim of this study is to further explore CEST at 2 ppm contrast of the human brain and

to investigate the metabolite correlates of CEST at 2 ppm through comparison with MRS measurements at 7T. First, we simulated the CEST effect based on Bloch-McConnell equations to determine ideal B_1 and saturation time settings. Hereafter, we imaged phantoms made of Cr solutions to validate the optimized CEST acquisition parameters *in vitro*. Since CEST contrast is influenced by temperature, we also scanned a phantom at both room and body temperatures to determine to what extent this variation could influence the contrast obtained. Finally, we investigated metabolite correlates of CEST at 2 ppm of the human brain *in vivo* via comparison with magnetic resonance spectroscopy (MRS). To achieve this goal, we scanned 10 healthy volunteers using a 7T human MRI system and examined the correlation between tCr obtained from MRS and CEST at 2 ppm. Differently from previous studies [66,88,92,99], we also assessed if Glu has a contribution to the CEST at 2 ppm contrast, given the broad effect of the CEST at 2 ppm pool, and the closely resonating CEST at 3 ppm pool. We further computed for the apparent exchange-dependent relaxation (AREX) employing a multi-pool Lorentzian fitting of the *in vivo* data. This approach aimed to correct for competing CEST effects and T_1 scaling. The goal was to see if statistical results differed from those obtained using the conventional MTR asymmetry metric.

4.3 Methods

4.3.1 Simulations

CEST from Cr in the human brain was simulated via Bloch-McConnell equations, using a five-pool model, including Cr, Glu, NOE, water and magnetization transfer (MT) pools. The goal was to simulate the CEST MTR asymmetry when using different total saturation time (t_{sat}) and B_1rms values, such that we could assess which parameter combination would yield maximum signal intensity. For each pool, we considered literature values of exchange rate constants, for spontaneous (k_0) and base (k_b) catalysis, respectively (Cr: k_0 = 0 Hz and $k_b = 7.81 \cdot 10^9$ Hz; Glu: $k_0 = 2.79 \cdot 10^3$ Hz and $k_b = 4.5 \cdot 10^{10}$ Hz; NOE: k_0 = 0 Hz and $k_b = 16 \cdot 10^7$ Hz) as well as T_2 values at 7T (Cr: 7.1 ms and Glu: 6.9 ms). Both metabolite concentrations were kept at 10 mM to mimic the approximate conditions in the human brain. For water, T_1 and T_2 were 1.6 s 62 ms respectively. Lastly, MT was simulated as a semi-solid pool given the very short T_2 times (± 10-5 s), thus we only considered its Z-magnetization[100].

4.3.2 Phantom preparation

Firstly, a phantom was prepared consisting of 10 vials of 60 ml each, which were placed in a glass container with Electronic Liquid FC-3283 (Fluorinert™, 3M™) embedding the tubes: (1) deionized water only, (2) a mixture of Cr (10 mM) and Glu (10 mM), (3-10) Cr or Glu with a range of concentration from 5 to 40 mM. Cr and Glu phantoms were made with N-Amidinosarcosine and L-Glutamic acid, respectively. Our objective was to establish a gradient of concentrations for the two metabolites, incorporating levels that closely approximate *in vivo* concentrations in the brain. Additionally, higher concentrations were included to evaluate the correlation between CEST and metabolites' concentration. Ultimately, the phantom was scanned at room temperature (21.5°C), at approximately 28°c**,** and finally at 36°C. The goal was to create a temperature gradient to observe how the CEST contrast would change as a function of temperature. Secondly, we prepared an additional phantom with 4 vials of 50 ml each. The goal was to match the metabolite concentration and correct for T_1 and T_2 relaxation times found in the human brain. These vials contained (1) deionized water, (2) 10 mM Cr and 10 mM Glu (3) 10 mM Cr and (4) 10 mM Glu, a range of concentration similar to previous studies[70]. A total 0.5 mM of $CuSO_4$ and 1% agarose were added for T_1 and T_2 adjustments[101]. Initial optimization of $CuSO_4$ and 1% agarose concentrations showed no significant contributions of these compounds to the Z-Spectra, except for an expected slight MT effect (Supplementary Figure S4). All vials were titrated to achieve a physiological pH of approximately 7.3 (± 0.05). Both phantoms were first heated up at the desired temperature on a hot plate, whereafter transferred into the scanner once the desired temperature was reached. To maintain the temperature constant while scanning, a water-circulating blanket was placed around the phantom container and connected to a Blanketrol III hyper-hypothermia system (Cincinnati Sub-Zero, Cincinnati, OH, USA). The temperature was monitored during image acquisition with an MRI compatible thermometer probe immersed in the Electronic Liquid FC-3283 or Fomblin® perfluoropolyether (PFPE)

medium surrounding the phantom tubes.

4.3.3 *In vivo* data collection

We included 10 healthy volunteers (8 Females, 2 Males; 31.7 ± 16 years). The study adhered to the local Institutional Review Board guidelines and approval. All participants gave written informed consent.

MRI scans were acquired using a whole body 7T Philips Achieva MRI scanner (Philips Healthcare, Best, The Netherlands) equipped with a dual-transmit and a 32-channel receiver head coil (Nova Medical Inc, Wilmington, MA, USA).

The acquisition protocol included a short survey scan, a sensitivity encoding (SENSE) reference scan, a B_0 map for third order B_0 shimming, a dual refocusing echo acquisition mode (DREAM) B_1 map to assess B_1 distribution and a water saturation shift reference (WASSR) scan for post-processing B_0 correction[102]. For B_1 inhomogeneity mitigation, we placed two dielectric pads on the right and left side of the head. The dielectric pads were custom made as previously described by Teeuwisse et al 2012[103,104].

4.3.3.1 CEST

The CEST imaging acquisition protocol was based on the outcome of the simulation and phantom studies and consisted of two CEST scans. Firstly, to achieve an optimal CEST at 2 ppm contrast, a pulsed CEST preparation of 20 sinc-gauss pulses of 50 ms with 25 ms interpulse delay (t_{sat} of 1500 ms) and a B_1rms of 2.14 μT was applied. Secondly, a pulsed CEST preparation of 20 sinc-gauss pulses of 40 ms with no interpulse delay (t_{sat} of 800 ms) and a B_1rms of 3.3 μT was used to achieve an optimal CEST at 3 ppm contrast. Differently from previous Glu-CEST experiments that were all performed with the same human 7T platform of a different vendor and predominantly on one site, the interpulse delays used in our work were required to adhere SAR and RF amplifier requirements of the scanner used in our study. A total of 22 frequencies were acquired with a step size of 136.4 Hz between -1500 Hz and 1500 Hz. CEST acquisition details regarding the scans initially performed in phantoms for optimization can be found in the Supplementary Table S1.

4.3.3.2 MR Spectroscopy

The MRS acquisition protocol consisted of a short semi-LASER scan with a TE of 34 ms and TR of 6000 ms, 32 single acquisitions and a B_1 amplitude of 18 μT. Water suppression was achieved using the variable pulse power and optimization relaxation delays (VAPOR) sequence. Frequency offset corrected inversion (FOCI) refocusing pulses were used to minimize in-plane chemical shift displacement errors. In total, four voxels-of-interest (VOIs) were acquired with

the following dimensions: 30 mm x 15 mm x 25 mm. VOIs were placed (1) in the frontal and posterior-cingulate cortex (PCC) to maximize gray matter (GM) content and (2) in the left and right parietal white matter (WM) to maximize WM content, with the effort to minimize partial volume effect. A visual representation of the VOIs planning can be found in Figure 3. For each VOI, a separate water reference scan was acquired (same acquisition parameters, 2 single acquisitions).

4.3.4 Data analysis

4.3.4.1 Anatomical images

3D T_1-weighted images were segmented into probabilistic tissue maps for WM, GM and cerebrospinal fluid (CSF) using FSL (Brain extraction Tool and FAST algorithm in the FMRIB Software Library)[78,79]. A custom-build MATLAB routine was then used to create binary tissue maps (values are either 0 or 1, with 1 given to the tissue with highest probabilistic value) and quantify the volume of each tissue type within each MRS VOI. Maps were also used to mask CEST images to account only for voxels with GM and WM content above 70% (and thus limit partial volume effect).

4.3.4.2 CEST

The WASSR data was used for B_0 inhomogeneity correction. B_1 corrections were done according to the method previously described[105]. The normalized, B_0 and B_1 corrected CEST images were then used to separately calculate the MTR asymmetry for 2 and 3 ppm CEST pools: $MTRasym = \frac{Z(-x\ ppm) - Z(+x\ ppm)}{Z(-x\ ppm)}$. We also fitted the data voxel wise to a five-pool Lorentzian model using the Levenberg-Marquardt algorithm[81]. More details can be found in the Supplementary Material. AREX was calculated per voxel as described in a previous publication[106].

The VOIs used for MRS acquisitions were used as masks to retrieve the CEST MTR asymmetry values.

4.3.4.3 MR Spectroscopy

Water-suppressed MRS spectra were corrected for eddy-currents and individual phase- and frequency-drift using a custom-built MATLAB routine and fitted with LCModel[107]. A basis-set was generated using the FID-A toolbox[108]. Non-water-suppressed data from same VOI were used for quantification. Water signal was corrected for GM, WM and cerebral spinal fluid (CSF) tissue fractions. Literature values for T_1 and T_2 relaxation time values of water in GM, WM and CSF as well as T_1 and T_2 relaxation time values of neurometabolites were used for correction[109.] Cramer-rao lower bounds (CRLBs) for total creatine (tCr = Cr + PCr) and Glu were obtained

from LCModel output. Individual water acquisitions were inspected for any large phase or amplitude drop (which could be explained with subject movement). For one dataset in the PCC we observed a large phase change in one of the single acquisitions and excluded it before averaging all other single acquisitions.

4.3.5 Statistical analysis

To evaluate the *in vivo* correlation between CEST and MRS results, we employed linear correlation, calculating the Pearson's correlation coefficient for both the CEST MTR asymmetry and AREX values, along with the metabolite concentrations obtained through MRS. For significance inspection we performed a student's t-test, setting the significance threshold at $p < 0.05$. Statistics were performed in R version 4.1.2 (R Core Team (2021).

4.4 Results

4.4.1 Simulations

Figure 1 illustrates the results of five-pool model simulations from CEST at 2 ppm for concentrations similar to those found in the human brain (10 mM) while taking the hardware limitations into account. The simulations showed that maximum CEST at 2 ppm value can be obtained with a t_{sat} of 1.5 s and a B_1rms of 2.5 μT or a t_{sat} of 1 s and a B_1rms of 3 μT. The areas in white on the right side of each map represent the acquisition parameter combinations that are not possible to achieve due to SAR and hardware limitations when imaging *in vivo*. In the Supplementary Figure S1A we show that as a comparison to CEST at 2 ppm, CEST at 3 ppm requires the maximum B_1rms possible, which was approximately 3.5 μT, and a somewhat shorter t_{sat} of 1 s.

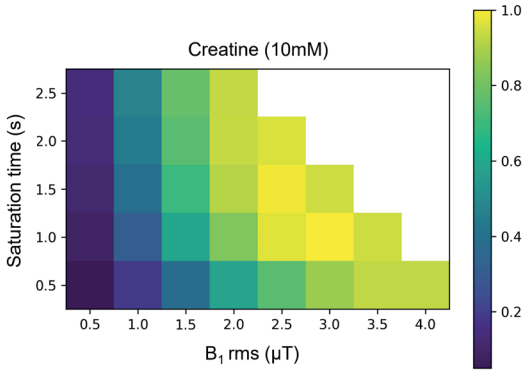

Figure 1. Normalized five-pool model simulation results. CEST MTR asymmetry was investigated as a function of varying B_1rms and t_{sat} to find the optimal acquisition values for CEST at 2 ppm CEST, corresponding to the CEST pools at 2 ppm. The areas on the right side in white of each figure, represent the parameter combinations which were not experimented due to SAR limitations *in vivo.*

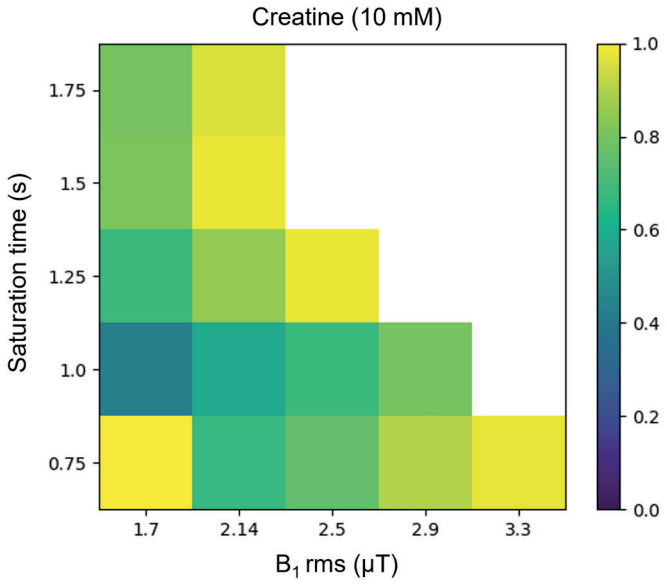

Figure 2. Phantom results normalized to the highest MTR asymmetry value. Maps illustrating how CEST at 2 ppm CEST changes as a function of total saturation time (s) and B_1rms (μT). The data shown corresponds to measurements of phantoms with a concentration of 10mM of creatine scanned at ± 36°C.

4.4.2 Phantoms

Figure 2 illustrates how CEST at 2 ppm changes *in vitro* at 36°C as a function of t_{sat} and B_1rms. Results at other temperatures can be found in Supplementary Figure S3. We wanted to specifically assess the optimal parameters to achieve maximum CEST contrast in an ideal experimental setting before applying it *in vivo*. Our results confirm that maximum CEST at 2 ppm was reached when using a t_{sat} = 1500 ms and a B_1rms of 2.14 μT. Unexpectedly, a t_{sat} of 750 ms and a B_1rms of 1.7 μT also yielded maximum CEST at 2 ppm. For CEST at 3 ppm, similarly to the literature, we found a t_{sat} of 750 ms and a B_1rms of 3.3 μT yielded the maximum MTR asymmetry (Supplementary Figure S1B). Additionally, we found temperature to have a linear relation with CEST at 2 ppm MTR asymmetry, where a physiological temperature yielded higher CEST contrast than at room temperature (Supplementary Figure S3A). Interestingly, for CEST at 3 ppm MTR asymmetry we observed the opposite, an inverse relation between temperature and MTR asymmetry (Supplementary Figure S3B).

4.4.3 Healthy volunteers

Figure 3 shows a representative example of how the MRS VOIs were planned in the GM and WM. The corresponding MR spectra are displayed for each VOI alongside the fitted signals of interest: tCr and Glu. Both metabolites could be measured and the results presented here represent reflect the average findings from all included subjects: a similar concentration of tCr

in WM (VOI1: 6.6 mM ± 0.4; VOI2: 6.6 mM ± 0.3) and GM (VOI3: 6.6 ± 0.7; VOI4: 6.6 mM ± 0.5), and a higher concentration of Glu in the GM (VOI3: 8.7 mM ± 0.7; VOI4: 8.3 mM ± 0.6) compared to the WM (VOI1: 6.5 mM ± 0.3; VOI2: 6.4 mM ± 0.6).

Figure 4 shows the average Z-Spectra and MTR asymmetry of CEST at 2 ppm of the voxels within the MRS VOI1 and VOI2 in the WM and VOI3 and VOI4 in the GM. The MTR asymmetry peak appears to be more evident in the GM voxels, whereas in the WM, there seems to be a greater contribution from NOE.

CEST maps at 2 ppm are displayed in Figure 5 for two representative subjects, with respective B_0 and B_1 maps. CEST at 2 ppm maps generally exhibit high values, especially in the GM, whereas susceptibility to B_1 inhomogeneity resulted in a loss of contrast in the anatomical right side of the brain. This phenomenon appears consistent across different subjects (Figures 5A and 5B). In contrast, we observed a more homogeneous B_1 distribution in the CEST at 3 ppm maps (Supplementary Figures S5A and S5B). Supplementary Figures S7A and S7B show AREX maps from CEST at 2 ppm, where higher values can be observed in the WM compared to the GM, as AREX represents an inverse metric of steady-state Z-spectra.

For both MTR asymmetry and AREX, CEST at 2 ppm value distributions from all 10 subjects are displayed for the VOIs placed in the WM and in the GM in Figures 6A and 6B and Supplementary Figure S8, respectively. CEST at 2 ppm MTR asymmetry values are broadly distributed, mostly between 0-20% in both GM and WM VOIs whereas the AREX values range between 0-80%. CEST at 3 ppm MTR asymmetry is mostly distributed between -10 and 5% in the WM and tends towards higher values in the GM (-10% to 10%) (Figures 6C and 6D). Intra-tissue distribution variability (i.e. VOI1 vs VOI2 or VOI3 vs VOI4) is observed for both CEST pools, for both CEST at 2 ppm and CEST at 3 ppm distributions in the GM and WM, with slightly less variation for CEST at 3 ppm contrast in the WM Figure 6C).

Figures 7A and 7B demonstrate the correlation between metabolite concentrations measured in the GM and WM and the corresponding CEST at 2 ppm MTR asymmetry values. Figure 7A shows a non-significant correlation between tCr and CEST at 2 ppm contrast ($R = 0.19$; p-value = 0.273). However, in Figure 7B, a significant correlation was found between CEST at 2 ppm and Glu concentration ($R = 0.39$; p-value = 0.033). We conducted similar comparisons for the AREX, an inverse metric of the Z-spectra, which also accounts for MT and T_1. In Figure 7C and 7D, similar to MTR asymmetry results, we found no correlation of AREX at 2 ppm and tCr ($R = 0.003$; p-value = 0.98) but an inverse significant correlation between AREX at 2 ppm and Glu ($R = 0.6$; p-value = 0.002). For internal validation, we also confirmed the significant correlation between the CEST at 3 ppm MTR asymmetry and Glu concentration ($R = 0.66$; p-value < 0.001) and did not find a significant correlation between CEST at 3 ppm MTR asymmetry and tCr ($R = 0.07$; $p = 0.681$) (Supplementary Figures 6SB and 6SA, respectively). Similarly, no correlation between CEST at 3 ppm and tCr was obtained using the AREX metric; however, also in this case, an inverse significant correlation between AREX at 3 ppm and Glu was obtained ($p = 0.010$; $R = 0.47$) (Supplementary Figures 6SC and 6SD).

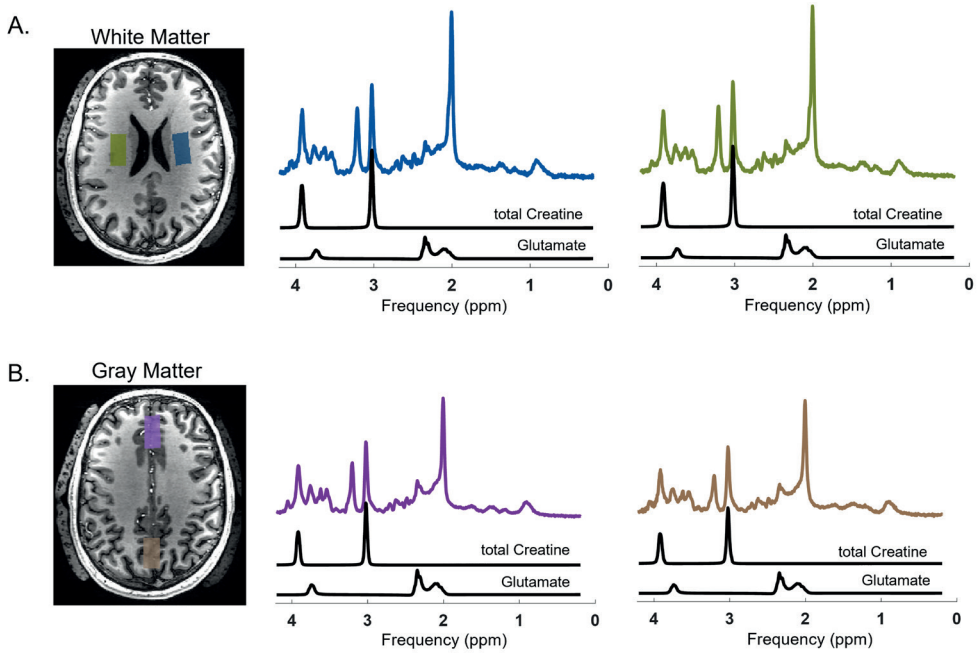

Figure 3. An example of how the MRS VOIs were planned and typical MRS results showing tCr and Glu fits from the WM (A) and from the GM (B). Outside of the skull area the dielectric pads can be seen.

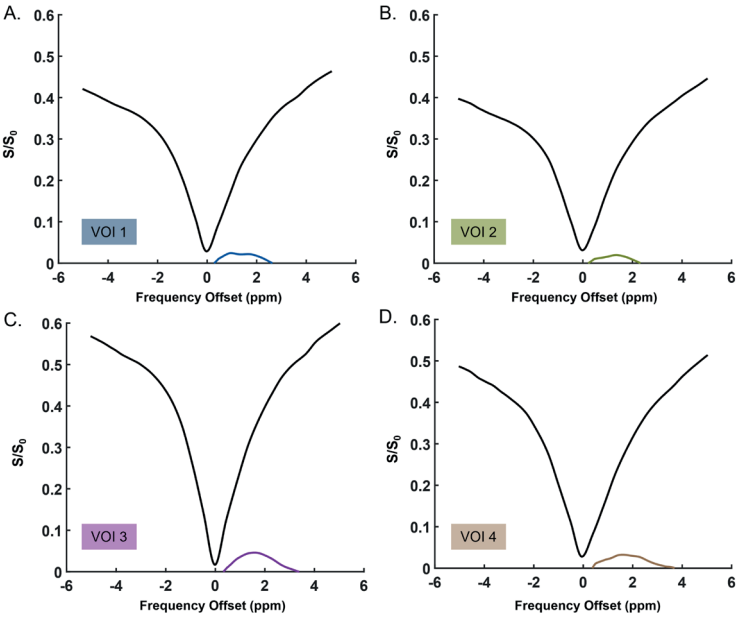

Figure 4. Average Z-Spectra and MTR asymmetry of the voxels in two VOIs in the White Matter (A & B) and Gray Matter (C & D). These results are from 1 representative volunteer.

4.5 Discussion and conclusions

The primary objective of our study was to further investigate CEST at 2 ppm in the human brain at 7T. Additionally, we conducted an internal validation of CEST at 3 ppm on a different 7T human MR platform than that predominantly used in previous studies in the literature. First, we identified optimal CEST at 2 ppm acquisition parameters in the human brain at 7T through simulations and confirmed them in phantoms *in vitro*. Subsequently, we evaluated the performance of the optimized sequences in the *in vivo* human brain using MRS as ground truth measurements of tCr and Glu concentrations. Our findings revealed a significant correlation between CEST at 2 ppm MTR asymmetry and Glu as measured by MRS, suggesting that glutamate is a substantial contributor to the observed CEST at 2 ppm contrast in the human brain. However, we did not observe a significant correlation between CEST at 2 ppm and Cr concentration in the brain.

Glutamate-weighted CEST imaging in the brain is gaining attention given its abundance and physiological role, supported by its visibility due to the presence of amine protons[88]. Because of the involvement of Glu in pathologies such as epilepsy, the use of CEST for Glu imaging at 7T has been explored in at least three previous studies[110–112]. Similarly, Cr is well known for playing an important role in tissue bioenergetics and is present in both muscles and brain aiding in adenosine triphosphate synthesis for cell energy requirements[113]. Cr, with its amine and guanidinium protons, is an interesting CEST contrast to be explored in *in vivo* human brain, especially considering its observed concentration changes in brain tumors[114]. Although both metabolites have amine protons, amines found in Glu resonate around 3 ppm from water with an exchange rate of approximately 5500 ± 500 Hz[88], while amines in Cr resonate around 2 ppm with an intermediate exchange rate of around 950 ± 100 Hz[70]. Their neighboring frequencies and the overlap between these two pools creates a challenge of specificity to each pool. Nevertheless, by taking advantage of the inherent differences in the exchange rates of amines in Glu and Cr, we determined via simulations the optimal saturation length and power to achieve maximum saturation efficiency for both metabolites separately, while accounting for SAR and hardware limitations of human MRI scanners. Consistent with a previous study, our simulation results (Figure 1) showed that an intermediate B_1rms with a long t_{sat} is essential to achieve maximum CEST at 2 ppm MTR asymmetry contrast. In the case of CEST at 3 ppm, our results corroborated previous findings on a human 7T system from a different vendor, emphasizing the need for a high B_1rms with a shorter t_{sat} is needed to achieve high CEST at 3 ppm contrast[66,99,115].

Via *in vitro* experiments, we validated the simulation results and determined the optimal RF power (B_1rms) and t_{sat} length to be: 2.14 µT & 1500 ms and 3.3 µT & 1000 ms , for CEST at 2 ppm and CEST at 3 ppm, respectively (Figure 2 and Supplementary Figure S1B, respectively). While one might argue, based on MTR asymmetry results (Figure 1), that choosing a higher B_1rms would be beneficial for CEST at 2 ppm, our assessment with the presence of glutamate, as expected in the human brain, revealed that a B_1rms of 2.5 µT and a t_{sat} of 1500 ms, would noticeably increase the contribution of CEST at 3 ppm (Supplementary Figure S2A). Interestingly,

a considerably high CEST MTR asymmetry was found in our phantoms with a low t_{sat} and B_1rms (750 ms and a B_1rms of 2.5 μT) (Figure 2). This observation, which is not supported by our simulations, could be attributed to field inhomogeneities, possibly induced by the movement of water within the heating blanket used during our measurements. Interestingly, a previous study which looked at CEST at 2 ppm fittings in the human brain showed a somewhat lower B_1rms of 1.45 μT and a slightly longer saturation duration of 2 s to be more beneficial for CEST at 2 ppm imaging[89]. However, the same study indicated that a B_1rms of 2 μT and total saturation of 2 s yielded comparable CEST at 2 ppm contrast to their suggested parameters (approximately 5% in the GM). Our simulation results did initially show the benefit of aiming for a slightly higher B_1rms of 2.5 μT or 3 μT, with t_{sat} set at either 1 s or 1.5 s, respectively. This is different from what we observed in phantoms, where the most optimal acquisition parameters were firstly a B_1rms of 2.14 μT with a t_{sat} of 1.5 s, and secondly a B_1rms of 2.5 μT with a t_{sat} of 1.25 s. The latter B_1rms is in line with what has been also recently shown to be optimal for CrCEST imaging in the mouse brain[99]. As for CEST at 3 ppm, the highest B_1rms of 3.3 μT with a t_{sat} of 1000 ms could not be reached within the SAR limitations. Consequently, for phantom experiments, we chose to reduce t_{sat} to 750ms and found the highest t_{sat} possible to be 750 ms while accommodating a B_1rms of 3.3 μT. *In vitro* studies in our work showed that the CEST contrast at 2 ppm and 3 ppm both increased with an increase in concentration (Supplementary Figure S3). Phantom experiments to validate metabolite-weighted contrast have been previously performed by Khlebnikov et al. 2019[66]. Differently from this work, our conclusions are also based on *in vivo* experiments. Our results indicate that hardware limitations need to be taken into account when developing and optimizing acquisition parameters, and emphasize the importance of choosing a concentration representative of physiological conditions to accurately mimic *in vivo* situations.

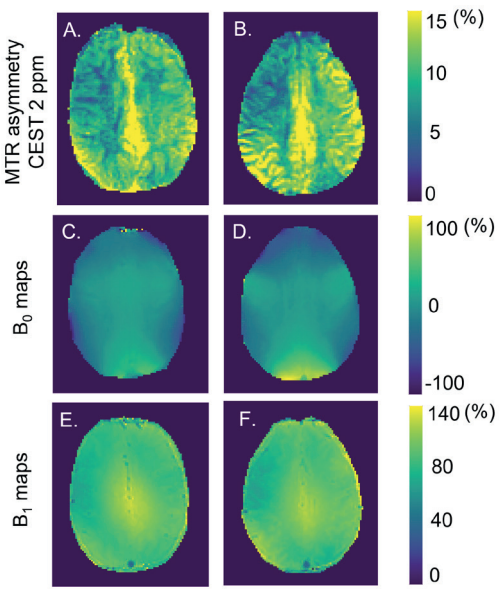

Figure 5. (A) & (B) CEST at 2 ppm MTR asymmetry maps of two representative subjects. (C) & (D) and (E) & (F) the corresponding B_0 and B_1 maps, respectively.

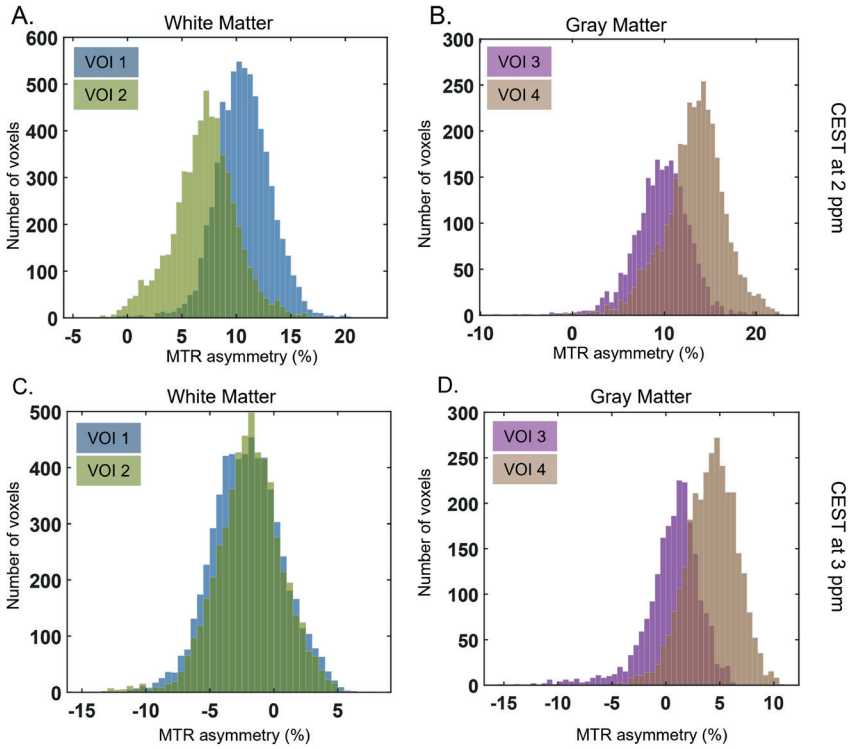

Figure 6. Histograms of the CEST MTR asymmetry contrast distribution from (A, B) CEST at 2 ppm and (C, D) CEST at 3 ppm in the VOIs placed in WM and GM, respectively. For each ROI the histogram reflects the average contrast across all 8 imaging slices from the 10 subjects combined.

To study the metabolite-weighted CEST contrast in the human brain, we applied CEST measurements using the optimized acquisition parameters and validated them against MRS. While many prior studies have applied specific CEST sequences to capture CEST at 3 ppm contrast, we have also included MRS for validation of CEST at 2 ppm in the GM and WM of multiple subjects, additionally to what has been previously done[89]. As expected, our results showed a significant correlation between Glu concentrations and CEST at 3 ppm MTR asymmetry (Supplementary Figure S6B). Surprisingly, we observed a significant correlation between CEST at 2 ppm and Glu concentrations, whereas no correlation was found between CEST at 2 ppm and tCr concentrations. The lack of correlation for CEST at 2 ppm could be attributed to different reasons. Firstly, the well-known similarity in Cr concentrations in the GM and WM limits the range over which the correlation could be assessed[116]. A potential future approach could include measurements in physiological conditions, such as during muscle exercise, where more pronounced tCr concentration changes are expected. Additionally, MRS measures tCr, therefore the phosphocreatine also contributes to the MRS measurements. The CEST contrast at 2 ppm is known to have PCr contribution around 80% in the rat brain with a saturation of 2 μT[117,118]. Although we know that the concentrations of Cr and PCr are comparable

in magnitude in the human brain, we do not know to in which proportions we are capturing the signal from Cr and/or PCr[119]. Differences in relative sensitivity to Cr and PCr could potentially play a role in correlating results from these two methodologies. Finally, the CEST contribution at 2 ppm can also include contrast from other proteins/peptides, from which some guanidinium protons contribution can arise as previously shown by Zhang et al[36]. On the other hand, the correlation of the CEST at 2 ppm pool with Glu concentrations could be due to contamination from the CEST at 3 ppm pool. It is known that this CEST pool can have a broad effect, especially in physiological temperatures. Moreover, Glu concentrations in the brain are higher than tCr, making it relatively easier to be more sensitive to the proton pool at 3 ppm. These results seem to suggest that the CEST MTR asymmetry contrast at 2 ppm is significantly influenced by Glu. On the other hand, when quantifying CEST with AREX, thus correcting for T_1 and MT effects, we found similar results for both CEST at 2 ppm and CEST at 3 ppm compared to MTR asymmetry (Figure 8 and Supplementary Figure S6). The observed inverse correlations were expected, as the AREX calculates the inverse Lorentzian difference[85]. The inverse CEST effect can also be seen in Supplementary Material Figure S7, where the WM appears more hyperintense than the GM, contrary to what we observed in MTR asymmetry maps (Figure 6A and 6B).

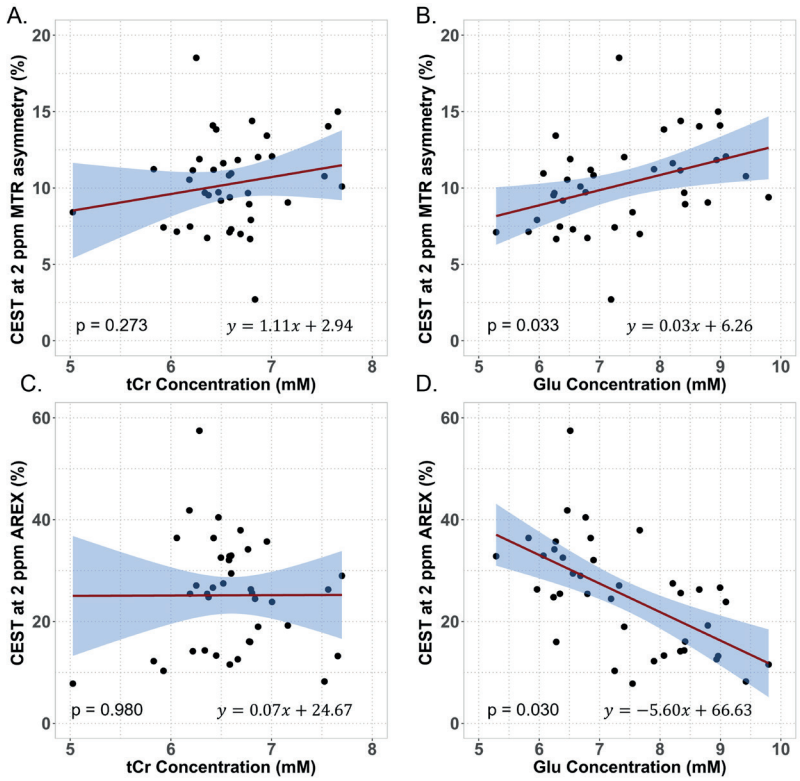

Figure 7. *In vivo* correlation results from data acquired with B_1rms = 2.14μT. Correlations of the (A,B) MTR asymmetry (p = 0.273, p = 0.033) and (C,D) AREX (p = 0.980, p = 0.030) of CEST at 2 ppm with tCr and Glu concentrations measured with MRS , respectively. The data plotted corresponds to 39 VOIs both in GM and WM as measured in 10 subjects.

Previous studies have shown the feasibility of CEST at 3 ppm imaging in the human brain at 7T[88,120]. Through simulations, *in vitro* experiments and measurements in healthy volunteers, we confirmed that the previously employed acquisition parameters also work on a different 7T platform than that used predominantly in the literature from a single center. By correlating the CEST at 3 ppm MTR asymmetry values with Glu concentrations, we can confirm that Glu is a substantial contributor to the CEST at 3 ppm contrast. Interestingly, a recent study has challenged the origins of the CEST contrast at 3 ppm, suggesting that it arises mainly from proteins rather than Glu in the rat brain[92]. Despite the difference in species, it is important to note that the data were acquired at a higher field strength than typically used in studies involving human subjects. Notably, the employed B_1 power was similar to our settings at 7T (3.6 μT), whereas previous simulations have shown that to achieve sensitivity to Glu at 9.4T a B_1 of around 7.5 μT would be optimal[66]. Additionally, simulations suggest that the CEST peak at 3 ppm becomes wider with increased B_0[49]. Consequently, the CEST contrast of proteins, which is typically observed around 3.5 ppm at 3T and 7T, might have also contributed to the observed effects around 3 ppm in that particular study.

When comparing the CEST contrast distributions within the two VOIs representing WM or GM for CEST at 2 ppm (Figures 6A and 6B), or even for CEST at 3 ppm (Figures 6C and 6D), the interregional spread is evident. These differences might be attributed to discrepancies in B_1 distribution within the brain illustrated in figures 5E and 5F (or Supplementary Figures S5E and S5F), even though for the vast majority of VOIs, the B_1 was above 80% (Supplementary Table S3). The B_1 differences predominantly appear as the systematic right-left variation, which reflect intraregional MTR asymmetry distribution in the WM VOIs (Figure 6A and 6C). We attempted to mitigate B_1 inhomogeneity effects by using dielectric pads during data acquisition and by applying a quadratic B_1 correction method[105]. The fact that the B_1 correction approach was originally developed for CEST at 3 ppm, which in principle uses a higher B_1 power value, might explain why it did not perform as effectively for the CEST at 2 ppm data. Furthermore, the uneven histogram distribution and negative values in WM could also be explained by contribution of other CEST effects such as magnetization transfer (MT) and nuclear Overhauser effect (NOE) to the MTR asymmetry. We would expect for the most part less contamination, especially when acquiring images with higher B_1rms (ie. filtering out other competing effects from slower exchanging pools such as NOE and amide protons). However, imperfect saturation and B_1 homogeneity distribution *in vivo* might have led to contamination to some extent throughout data acquisition, becoming more noticeable when combining data from all volunteers. Other analysis methods such as Lorentzian fittings could be considered as a good alternative for filtering out prominent competing effects *in vivo*[121,122]. After performing these fits, we computed the AREX metric accounting for T_1 and MT, but still observed an uneven distribution of the CEST contrast (Supplementary Material Figure S8). This could perhaps be due to field inhomogeneities, or challenges arising from fitting broad CEST pools. Consequently, contamination by neighboring pools may result in the interference of undesired CEST effects, as exemplified in one volunteer in Supplementary Material Figure S7. Our results in Supplementary Material Figure S9 show how broad the CEST at 2 ppm and CEST at 3 ppm

fittings are within the frequency spectrum, in line with a previous observation that the CEST contrast from fast exchanging components does not follow Lorentzian line shapes[123]. This has also been previously described in literature suggesting[41,42] that, because of the rather wide CEST at 3 ppm effect at physiological pH, fitting Lorentzians is particularly challenging because of the very wide peak[124]. Xu et al. discuss that the specificity of performing Lorentzian fittings improves CEST at 2 ppm quantification and that Cr and PCr pools could be extracted from animal muscle[118]. However, the concentration of these metabolites in muscle is higher than in the brain, and studies supporting this claim have been conducted at 11.7T, allowing for a higher spectral resolution than at 7T[125–127].

In addition to the B_1 inhomogeneities, our study has a few other limitations. An interesting cofounder affecting *in vitro* experiments for CEST at 3 ppm contrast seems to be temperature. We observed CEST at 2 ppm and CEST at 3 ppm contrasts to have a linear and inverse relation with temperature, respectively (Supplementary Figure S3B), as also shown in a zebrafish model for CEST at 3 ppm[128]. Lastly, since this investigation primarily served as a proof of principle for CEST at 2 ppm, our conclusions are limited by the relatively small sample size of 10 subjects, all of whom were healthy. However, the subjects spanned a relatively wide age range, which might have helped to study the CEST contrasts over different metabolite concentrations, since it is known that metabolite concentration in the brain changes with age[129].

In conclusion, we investigated optimal acquisition parameters for metabolite CEST imaging through simulations and validated these concepts in a controlled *in vitro* environment. We confirmed the significant contribution of Glu to the CEST at 3 ppm MTR asymmetry in vivo. Contrary to expectations, we observed that the CEST at 2 ppm pool is significantly correlated with Glu concentrations, indicating that the contrast is likely weighted by Glu. Our findings suggest that Glu is a substantial contributor to the CEST at 2 ppm contrast observed in the human brain, whereas the Cr contribution to CEST at 2 ppm in the brain did not exhibit a significant impact. A potentially interesting future step could involve applying a similar protocol in muscle imaging to assess whether CEST at 2 ppm can be validated in the presence of a larger concentration of Cr protons. Furthermore, it would be valuable to verify these sequences in pathologies such as brain tumors, expanding on the work of Cai et al.[63]. This way, the specificity of metabolite-weighted CEST could be reliably validated for future clinical applications.

4.6 Acknowledgments

This study is part of the project “Non-Invasive Characterization of Active Multiple Sclerosis Lesions Through Chemical Exchange Saturation Transfer (CEST) Imaging” (project no. 16862) financed by the Dutch Research Council (NWO) Talent Programme Veni. This work was also funded by the Medical Delta Cancer Diagnostics 3.0 program.

We would like to thank Wyger Brink for making the dielectric pads we used and supporting us while tackling B_1 constraints during protocol optimization. We would also like to thank Emiel

C.A. Roefs with the support while finetuning the analysis pipeline and with adjusting the T_1 and T_2 of the phantoms.

4.7 Conflict of interest

Ece Ercan is a full-time employee at Philips Healthcare, Best, The Netherlands.

4.8 Supplementary material

In vivo data analysis to calculate AREX:

For each voxel, Z-spectra was fitted to a five-pool Lorentzian model using the Levenberg-Marquardt algorithm. The model included the water, MT, relayed nuclear Overhauser effect (rNOE), amines at 2 ppm and amines at 3 ppm[130]. The fitting parameters can be found in the supplementary material under Table S2. Hereafter the relaxation compensated (AREX) contrast was calculated per voxel, also correcting for direct water saturation, MT and T_1: $AREX = \frac{\frac{1}{Z_{lab}} - \frac{1}{Z_{ref}}}{T_1}$, where Z_{lab} is the yielded label Z-spectrum and Z_{ref} is a reference spectrum given by $Z_{ref} = Z_{lab} + L_{pool}$, where L_{pool} is the Lorentzian dedicated to a specific pool at a certain resonance frequency (in ppm).

Supplementary Table S1. Acquisition parameters from phantom scans acquired during protocol optimization.

	Phantom image acquisition parameters
Shot TR/TR/TE (s)	5 / 3.3 / 1.82
Field of view (FOV (mm^3)	246 x 246 x32
Voxel size (mm^3)	2 x 2 x 4
Radiofrequency (RF) pulses	Sinc gauss
Frequency steps (Hz)	22 steps of 136.4
Frequency offset (Hz)	-1500Hz to 1500
Frequencies (ppm)	5, 4.54, 4.08, 3.62, 3.16, 2.7, 2.24, 1.78, 1.32, 0.86, 0.46, 0, -0.46, -0.86, -1.32, -1.78, -2.24, -2.7, -3.16, -3.62, -4.54, -5
B_1 rms (µT)	1.7, 2.1, 2.5, 2.9, 3.3
RF pulse duration/interval/repetition	50ms/25ms/10 | 50ms/0ms/20 | 75ms/50ms/10 | 50ms/25ms/20 | 100ms/75ms/10
RF total saturation duration (ms)	750 / 1000 / 1250 / 1500 / 1750

Supplementary Table S2. Table showing the actual average (Act avg) B_1 measured in each VOI for CEST at 2 ppm MTR asymmetry (Act avg B_1 2 ppm) and for CEST at 3 ppm MTR asymmetry (Act avg B_1 3 ppm), the MTR asymmetry values for both CEST contrasts and corresponding metabolite concentrations measured with MRS. For volunteer 9 the metabolites in VOI3 could not be measured (CRLB > 10%).

VOI	VOI1						VOI2					
Measurements	**CEST measurements**				**MRS measurements**		**CEST measurements**				**MRS measurements**	
Volunteers	Act avg B_1 CEST at 2 ppm (µT)	CEST at 2 ppm MTRasym (%)	Act avg B_1 CEST at 3 ppm (µT)	CEST at 3 ppm MTRasym (%)	Total creatine (mM)	Glutamate (mM)	Act avg B_1 CEST at 2 ppm (µT)	CEST at 2 ppm MTRasym (%)	Act avg B_1 CEST at 3 ppm (µT)	CEST at 3 ppm MTRasym (%)	Total creatine (mM)	Glutamate (mM)
Volunteer 1	1.9	10.1	3.5	-2.2	7.7	6.7	1.8	7.5	3.3	-1.0	6.2	6.3
Volunteer 2	1.9	10.5	3.3	-2.2	6.2	6.5	1.7	7.0	3.0	-1.0	6.7	7.7
Volunteer 3	2.4	11.9	3.7	-1.2	6.3	6.5	2.7	7.9	3.5	-0.2	6.8	6.0
Volunteer 4	2.0	9.5	3.4	-1.1	6.4	6.2	1.8	6.7	3.0	-3.5	6.8	6.3
Volunteer 5	2.1	11.0	3.5	-3.6	6.6	6.1	1.9	7.3	3.2	-0.2	6.6	6.6
Volunteer 6	2.2	13.4	3.7	-0.1	7.0	6.3	1.9	9.7	3.3	-0.5	6.8	6.3
Volunteer 7	2.1	10.8	3.6	-1.8	6.6	6.9	1.8	6.7	3.1	-1.0	6.4	6.8
Volunteer 8	2.2	9.7	3.3	-2.7	6.5	6.8	1.7	2.7	2.6	-4.5	6.8	7.2
Volunteer 9	2.0	11.2	3.4	0.0	6.4	6.9	1.9	7.1	3.2	-1.8	6.1	5.8
Voltuneer 10	1.9	9.2	3.0	-2.8	6.5	6.4	1.8	7.1	2.8	-2.9	6.6	5.3

VOI	VOI3						VOI4					
Measurements	**CEST measurements**				**MRS measurements**		**CEST measurements**				**MRS measurements**	
Volunteers	Act avg B_1 CEST at 2 ppm (μT)	CEST at 2 ppm MTRasym (%)	Act avg B_1 CEST at 3 ppm (μT)	CEST at 3 ppm MTRasym (%)	Total creatine (mM)	Glutamate (mM)	Act avg B_1 CEST at 2 ppm (μT)	CEST at 2 ppm MTRasym (%)	Act avg B_1 CEST at 3 ppm (μT)	CEST at 3 ppm MTRasym (%)	Total creatine (mM)	Glutamate (mM)
Volunteer 1	1.8	11.8	3.3	1.7	6.7	8.9	2.0	13.8	3.6	3.4	6.5	8.1
Volunteer 2	1.8	8.9	3.1	0.6	6.8	8.4	2.0	14.1	3.6	3.5	6.4	9.0
Volunteer 3	2.2	11.2	3.4	0.2	6.2	8.3	2.4	12.1	3.7	3.3	7.0	9.1
Volunteer 4	1.8	8.4	3.0	-1.0	5.0	7.5	2.1	11.2	3.4	2.4	5.8	7.9
Volunteer 5	2.1	9.0	3.5	1.0	7.2	8.8	2.1	12.0	3.6	1.2	6.9	7.4
Volunteer 6	2.0	11.6	3.5	1.1	6.5	8.2	2.2	18.5	3.8	4.1	6.3	7.3
Volunteer 7	1.7	10.8	2.9	0.4	7.5	9.4	2.1	15.0	3.6	1.3	7.7	9.0
Volunteer 8	2.0	9.4	3.1	0.3	6.6	9.8	1.9	9.7	3.0	0.5	6.3	8.4
Volunteer 9	1.7	9.2	2.9	-0.5			2.2	14.4	3.7	3.2	6.8	8.3
Voltuneer 10	1.8	7.4	2.9	0.2	5.9	7.2	2.1	14.0	3.4	2.2	7.6	8.6

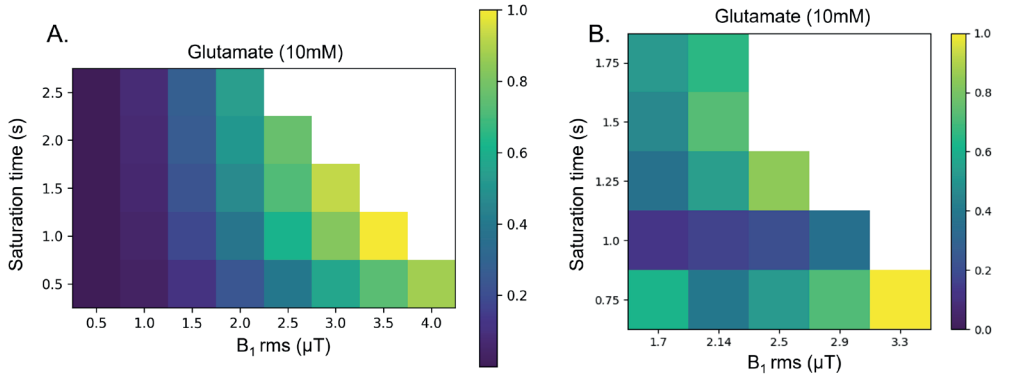

Supplementary Figure S1. (A) Normalized five-pool model simulation results normalized to the maximum CEST at 3 ppm MTR asymmetry value. investigated as a function of varying B_1rms and t_{sat} values. The areas on the right side in white of each figure, represent the parameter combinations which were not measured due to SAR limitations *in vivo.* (B) Phantom results normalized to the highest CEST at 3 ppm MTR asymmetry value, illustrating how CEST at 3 ppm CEST changes as a function of total saturation time (s) and B_1rms (μT). The data shown corresponds to measurements of phantoms with a concentration of 10mM of glutamate scanned at ± 36°C.

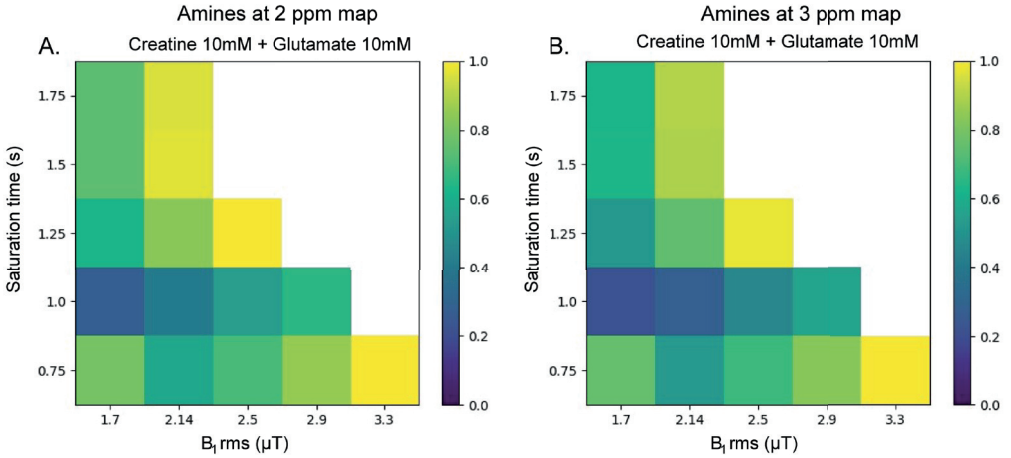

Supplementary Figure S2. Normalized phantom results to the maximum MTR asymmetry value. CEST MTR asymmetry was investigated as a function of varying B_1rms and t_{sat} values for (A) CEST at 2 ppm and (B) CEST at 3 ppm in a phantom, when in the presence of both creatine and glutamate. The areas on the right side in white of each figure, represent the parameter combinations which were not experimented due to SAR limitations *in vivo.*

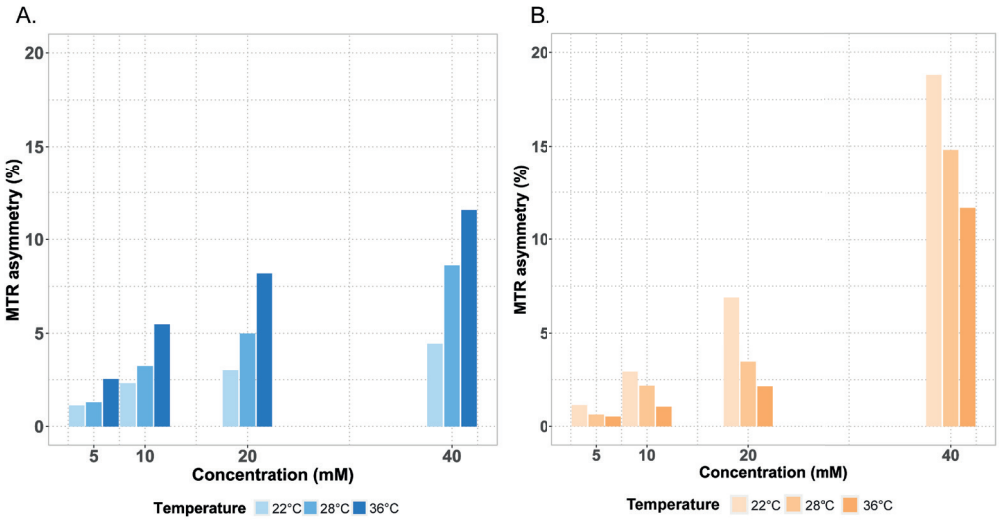

Supplementary Figure S3. Bar graph illustrating how the MTR asymmetry of (A) CEST at 2 ppm and (B) CEST at 3 ppm phantoms changed between three different temperature conditions. These scans were acquired with the parameters determined to be most optimal for 2 ppm and 3 ppm, respectively. It is evident that the CEST signal increases with temperature for CEST at 2 ppm and decreases for CEST at 3 ppm.

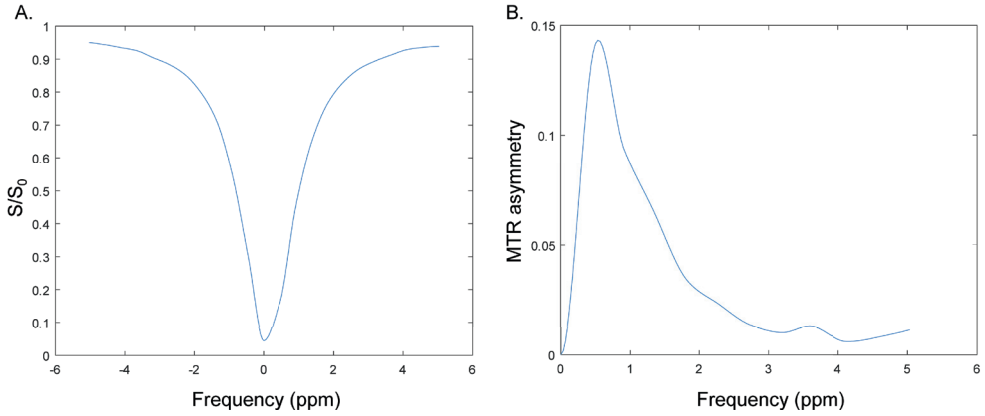

Supplementary Figure S4. (A) Z-Spectra and (B) MTR asymmetry from an ROI placed over a phantom with 0.5mM $CuSO_4$ and 1% agarose. This experiment was part of the initial optimization performed to determine the optimal concentrations to reach T_1 and T_2 relaxation times similar to those found in the human brain. The graphs shows that, except for MT effect, there are no heavy contributions of the compounds used to the Z-Spectra and MTR asymmetry.

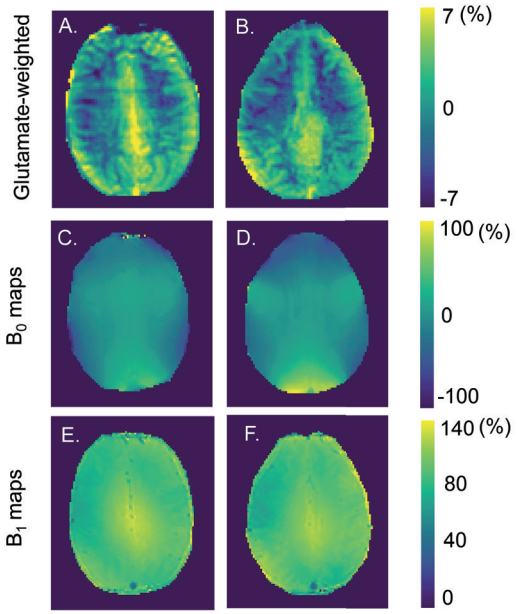

Supplementary Figure S5. (A) & (B) CEST at 3 ppm MTR asymmetry maps of two representative subjects. (C) & (D) and (E) & (F) the corresponding B_0 and B_1 maps, respectively.

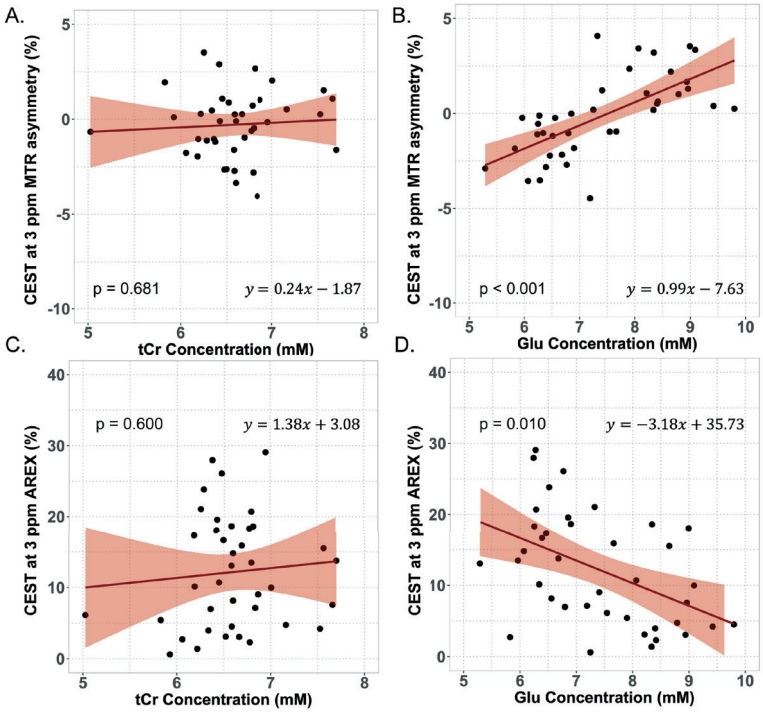

Supplementary Figure S6. *In vivo* correlation results from data acquired with B_1rms = 3.3μT. Correlations of the (A,B) MTR asymmetry (p = 0.681, p < 0.0.001) and (C,D) AREX (p = 0.600, p = 0.010) of CEST at 3 ppm with tCr and Glu concentrations measured with MRS, respectively. The data plotted corresponds to 39 VOIs both in GM and WM as measured in 10 subjects.

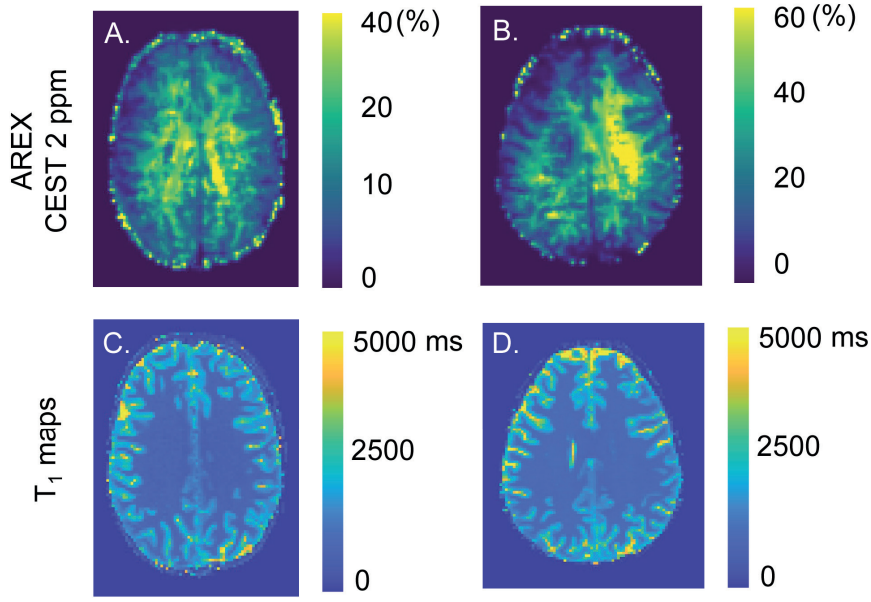

Supplementary Figure S7. (A) & (B) AREX maps of CEST at 2 ppm of two representative subjects. (C) & (D) the respective T_1 maps.

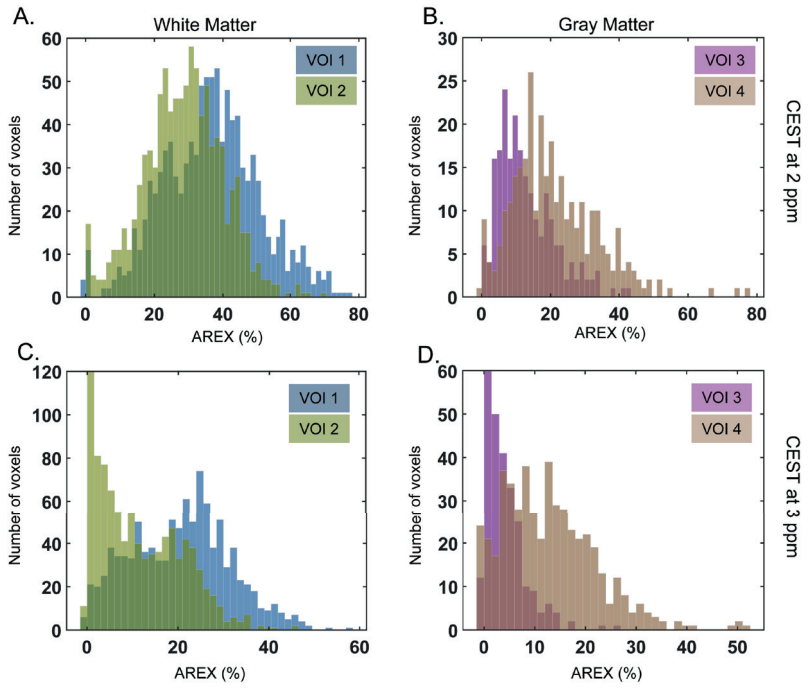

Supplementary Figure S8. Histograms of the CEST AREX contrast distribution from (A, B) CEST at 2 ppm and (C, D) CEST at 3 ppm in the VOIs placed in WM and GM, respectively. For each ROI the histogram reflects the average signal across all 8 imaging slices from the 10 subjects combined.

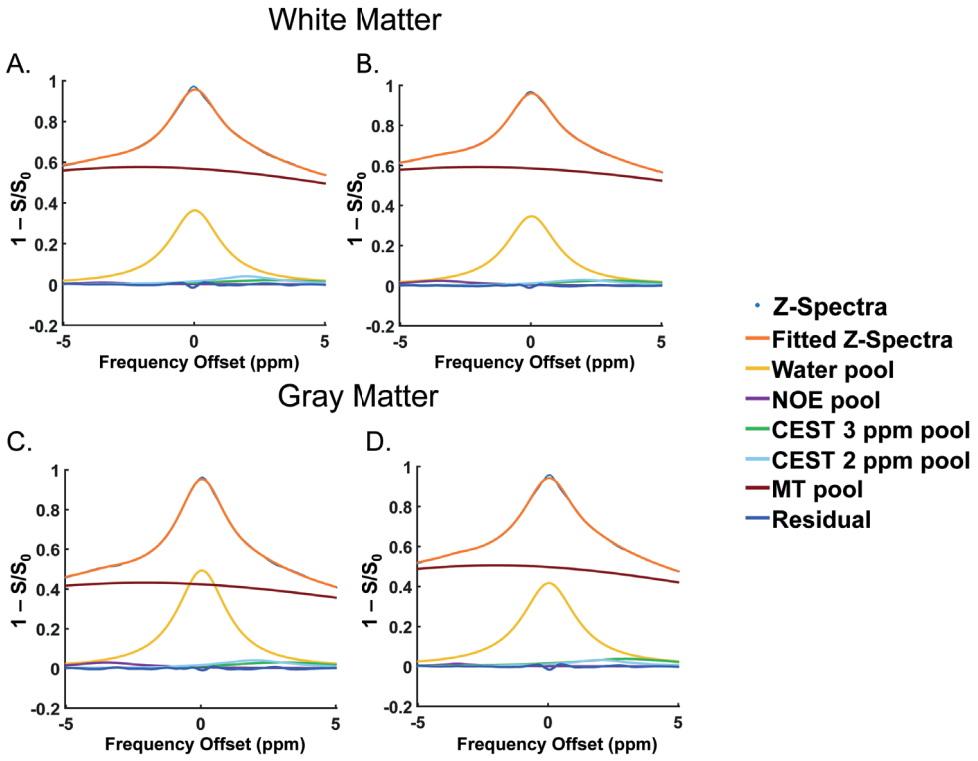

Supplementary Figure S9. Z-Spectra and five CEST pools fitted with Lorentzian line shapes from two VOIs in the WM (A & B) and GM (C & D). These results are from 1 representative volunteer.